FE analysis for estimating geotechnical parameters in liquefied sand from pile load test results

H. H. Tamboura
Chief, Scientific Research Section, GIKEN LTD., Kochi, Japan
Y. Ishihara
Manager, Scientific Research Section, GIKEN LTD., Kochi, Japan
K. Toda
Chief, Scientific Research Section, GIKEN LTD., Kochi, Japan
A. Burakowski
Student, Department of Engineering, University of Cambridge, Cambridgeshire, UK
S. K. Haigh
Professor, Department of Engineering, University of Cambridge, Cambridgeshire, UK

ABSTRACT

The study aims to achieve a valid numerical analysis method for estimating the geotechnical parameters of liquefied sand in "Liquefaction Test Apparatus" based on Cone Penetration Test (CPT) results and FE analysis simulating static load test results on a single square pile. The study is built upon the experimental study that simulated Liquefaction in "Liquefaction Test Apparatus", with CPT and large-scale pile load tests conducted during the liquefaction phase. These tests encompassed various excess pore water pressure ratio values (r_u= 0; 0.3; 0.6; and 0.9). In the present study, for each r_u value, soil parameters to be used in the numerical analyses were estimated using the CPT test results, followed by numerical analyses to scrutinize the vertical and horizontal pile capacities. The investigation explored the relationships between r_u and soil parameters, as well as their influence on bearing capacity. The large-scale pile vertical and horizontal load test results at r_u= 0 were successfully reproduced by the numerical analyses, confirming the validity of the used numerical model. The pile's vertical and horizontal capacities were then estimated for each r_u value (r_u= 0; 0.3; 0.6; and 0.9). The numerical analyses were confirmed to reproduce the experimental trend of a roughly linear decrease in soil parameters and bearing capacity as the r_u increased.

Keywords: *Liquefaction, Cone Penetration Test, Soil Parameters, Pile Bearing capacity, Numerical Analysis*

1. Introduction

Liquefaction poses a significant threat to foundations, diminishing their bearing capacity. In response, GIKEN has actively explored methods to enhance foundation stability in liquefiable soils, proposing various pile-supported structures Ishihara et al. (2023); Willcocks, (2021). A notable advancement is GIKEN's unique large-scale Liquefaction apparatus, employing water pumps to replicate liquefaction effects. This apparatus, featuring water pipes beneath it, enables the creation of excess pore water pressure, simulating liquefaction conditions (**Fig. 1**).

Numerical analysis, a potent tool for studying pile behaviors, relies on appropriate interface elements for accurate soil-pile interaction replication. MIDAS GTS NX, a widely used software, is instrumental in exploring complex pile-soil dynamics. Tamboura et al. (2024) proposed equations to derive effective interface elements based on load settlement curves, ensuring faithful reproduction of soil-pile interaction phenomena in MIDAS GTS NX.

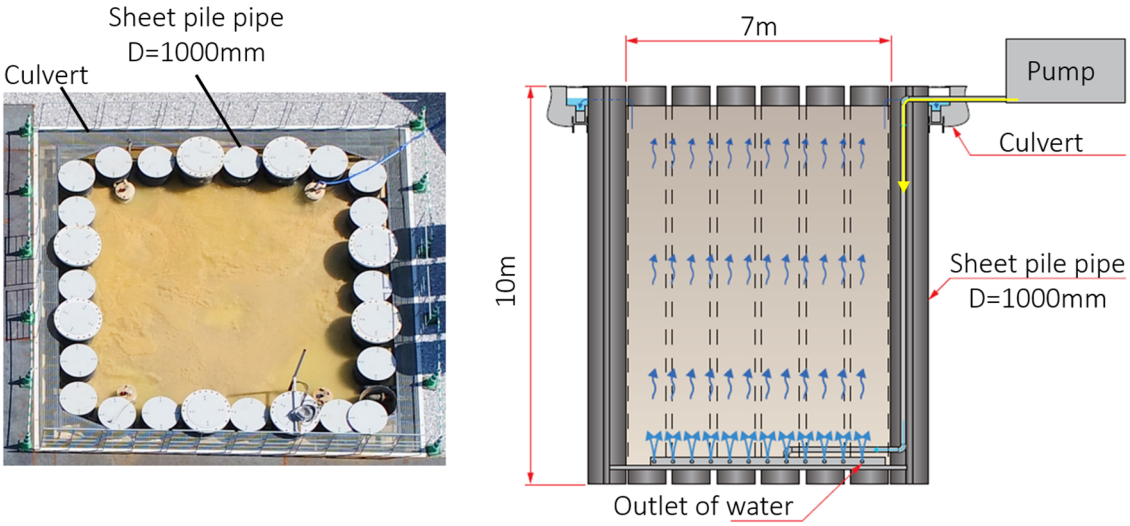

(a) Photo (**Top** view) **(b)** Schemas of vertical sectional view

Fig. 1 Liquefaction apparatus (After Toda et al. 2024)

Valuable insights from Robertson and Cabal (2010), Robertson and Campanella (1983), Kulhawy and Mayne (1990), and Robertson (2009) significantly contribute to unraveling the intricate relationships between CPT results and soil parameters. These studies provide essential knowledge for accurate geotechnical assessments and form a crucial foundation for interpreting CPT data in the context of soil behavior.

Building on the work of Toda et al. (2024), the current study aims to achieve a valid numerical analysis method to reproduce their experimental results, by exploring relationships between excess pore water pressure ratios (r_u) and soil parameters obtained through CPT Data interpretations, elucidating their impact on pile-bearing capacity. Numerical analysis, utilizing MIDAS GTS NX software, will be employed, leveraging equations proposed by Tamboura et al. (2024) to model effective soil-pile interaction.

2. Large-scale liquefaction tests of Toda et al. (2024)

2.1. Outline of the large-scale tests

Some soil specifications at the initial condition of the soil are shown in **Table 1** and **Fig. 2** shows the particle size distribution.

In the study of Toda et al. (2024) a square steel pile installed in the Liquefaction apparatus (**Fig. 1**) underwent both vertical and horizontal loading tests, varying the excess pore water pressure (Δ_u) for different assessments. Earth and water pressure sensors, detailed in **Fig. 3**, were strategically placed on the ground and the pile, alongside the locations of CPTs. Calibration was initially conducted to correlate the volumetric flow rate of pumps with the excess pore water pressure ratio (r_u). Subsequently, CPTs were executed at varying volumetric flow rates corresponding to r_u values of 0, 0.3, 0.6, and 0.9, utilizing a CPT device as depicted in **Fig. 4a**. The obtained CPT results will be instrumental in investigating the impact of liquefaction on soil parameters in the present study.

For pile installation, the soil was fully liquefied, and the pile, akin to the non-displacement pile, was inserted under gravity's influence. **Fig. 4b** illustrates the pile installation process, with **Table 2** specifying the pile parameters. Post-installation, liquefaction ceased, followed by water drainage and a 24-hour curing period. Subsequently, vertical and horizontal loading tests were conducted under specified r_u, as captured in **Fig. 4c**. The vertical tests were conducted first. After each test, the pile was removed and the soil condition was rearranged.

2.2. Large-scale test results

During the calibration phase without the pile, **Fig. 5a.** illustrates measured pore water pressures at various depths (1 m, 3 m, and 5 m) on both the North and South sides of the liquefaction apparatus. The results, denoted as WN1, WN3, WN5 for the North side, and WS1, WS3, WS5 for the South side, exhibit linear increases over time, correlating with the volumetric flow rate rise due to pump activity. The calculated r_u(r_u= Δ_u/σ'; Δu = measured

Table 1. Soil specifications at the initial condition

Soil particle density (ρ_s) [g/cm^3]	Minimum density ρdmin (ρ_{smin}) [g/cm^3]	Maximum density ρdmax (ρ_{smax}) [g/cm^3]	Maximum void ratio (e_{max})	Minimum void ratio (e_{min})	Classification	Density (ρ) [g/cm^3]	Relative density (D_r) [%]	Hydraulic conductivity (k) [m/s]
2.634	1.393	1.721	0.891	0.531	(SP)	1.6	67.88%	9.63E-5

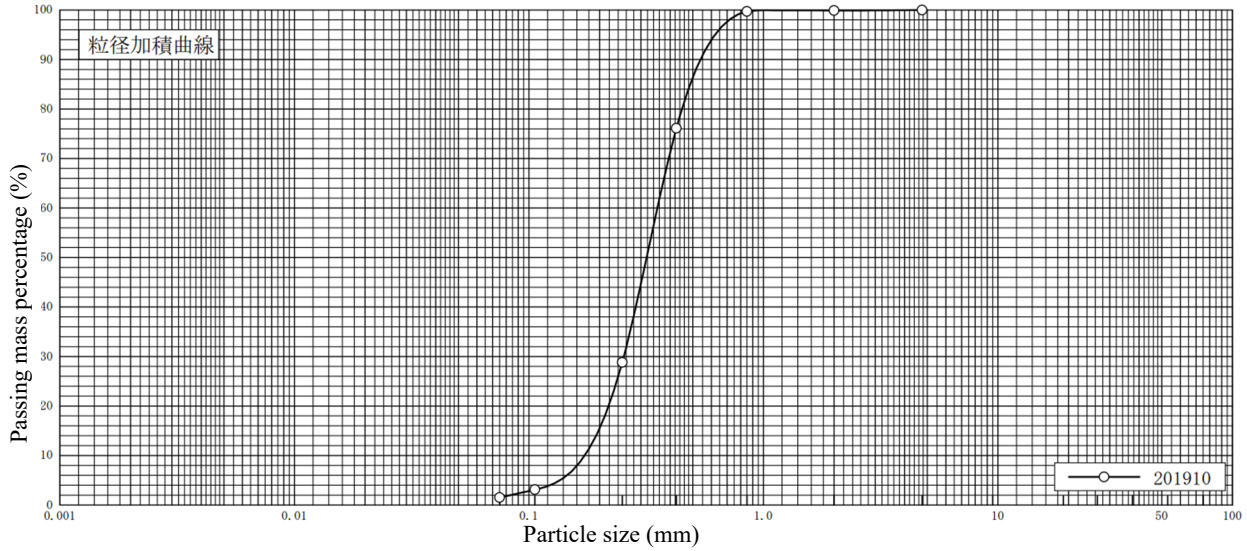

Fig. 2 Particle size distribution

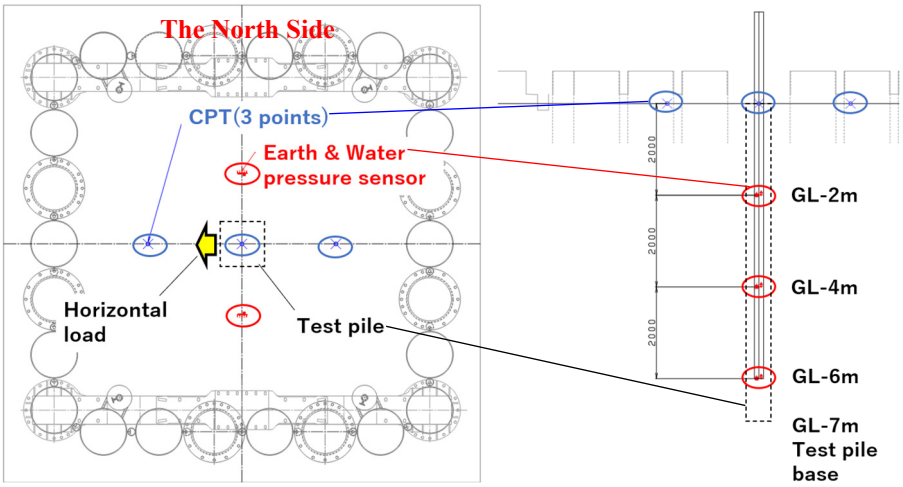

(a) Plan view **(b)** Sectional view

Fig. 3 Measurement outline (After Toda et al. 2024)

Table 2. Properties of prototype piles.

Type	Width [mm]	Thickness [mm]	Total Length [mm]	Embedded Length [mm]	Sectional area, [cm^2]	Second moment of area, I [cm^4]
Square Closed End Pile	300	9	8945	7045	102	14200

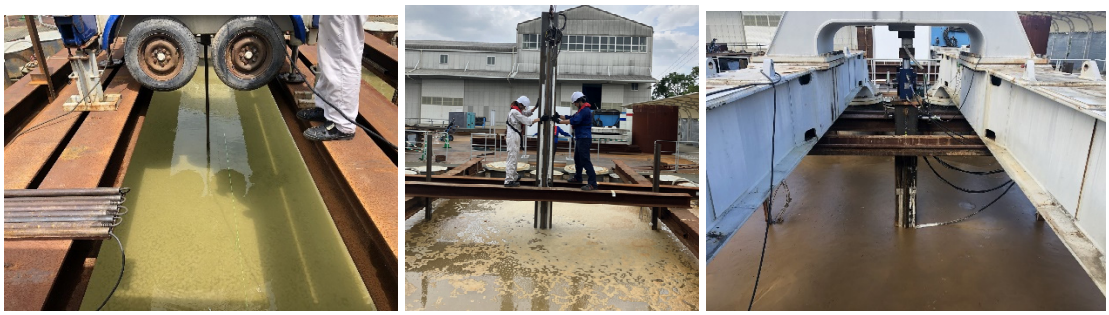

(a) CPT (case of r_u= 0.3) **(b)** Pile installation **(c)** Vertical loading test (r_u= 0)

Fig. 4 Some photos of the experiment in the liquefaction apparatus

excess pore pressure and σ' = initial effective stress) are shown in **Fig. 5b**. The discrepancies, at 1 m depth, are attributed to the turbulent movement of the soil particles at the upper part of the liquefaction apparatus after fluidization. Hence, the depths 3 m and 5 m were considered to control the r_u for CPT. **Fig. 5c** establishes the relationship between pump volumetric rate and r_u, enabling precise r_u control in the apparatus.

The penetration rate of the CPT was set at 2 cm/s. The CPT results in **Fig. 6** reveal decreasing cone resistance and friction with rising r_u, reaching zero friction at r_u= 0.9 due to full soil fluidization. Depth-wise, the upper 3 m is relatively softer. **Fig. 7** illustrates load-settlement curves for vertical and horizontal loading pretests at r_u = 0, pinpointing a vertical capacity of 160 kN and horizontal capacity of 53 kN at 10% pile diameter displacement. The pile was removed and reinstalled after each test. Despite the rearrangements of soil condition, these multiple pile installations at the same position impacted the soil strength, leading to considering only the r_u= 0 case as a reference in the present study after conducting thorough loading tests.

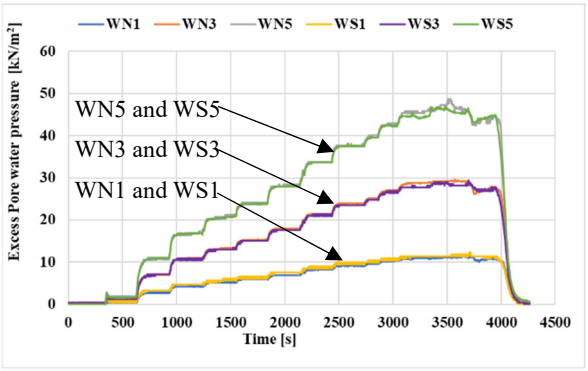

(a) Variation of excess pore water pressure with time

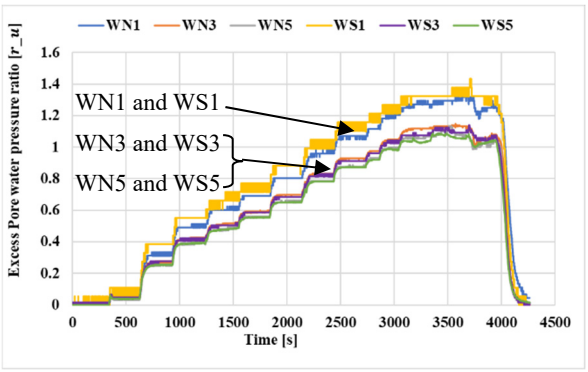

(b) Variation of r_u according to time

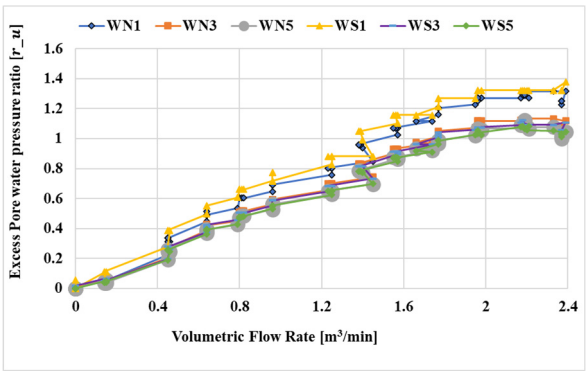

(c) Variation of r_u according to the pump's flow rate

Fig. 5 Calibration of the pumps and r_u (After Toda et al. 2024)

3. Soil parameter from CPT data interpretation

Robertson and Cabal (2010) delved into soil unit weight estimation based on CPT results and introduced a formula for this purpose. The formula, as proposed by Robertson and Cabal (2010), correlates soil unit weight with the friction ratio and cone resistance, expressed in **Eq. (1)**. This study adopts this relationship to calculate the soil unit weight.

$$\gamma/\gamma_w = 0.27(\log R_f) + 0.36\left[\log\left(\frac{q_t}{P_a}\right)\right] + 1.236 \quad (1)$$

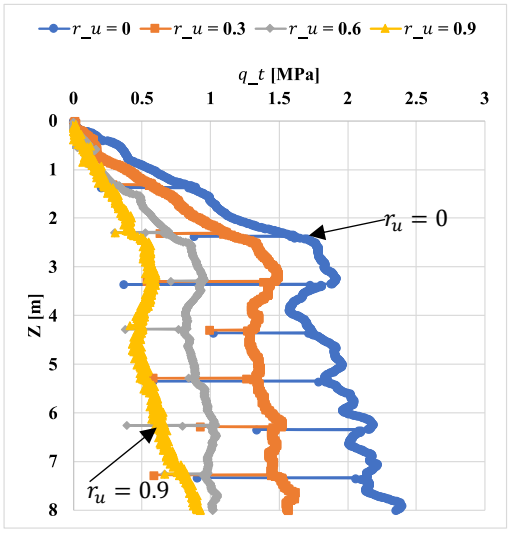

(a) Corrected cone resistance

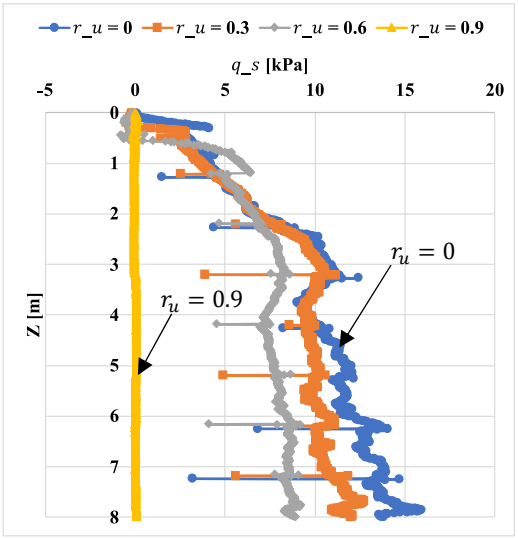

(b) Sleeve friction

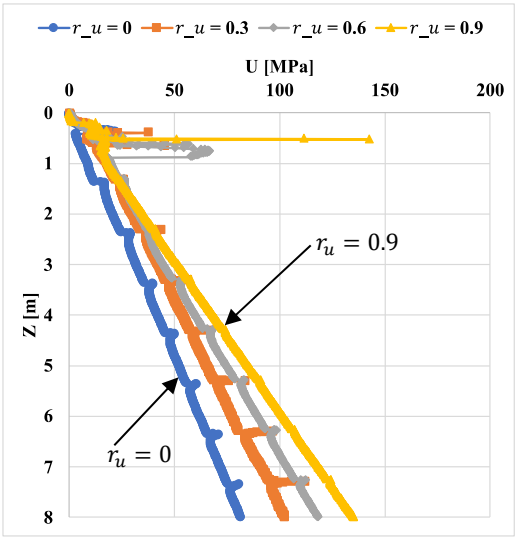

(c) Excess pore water pressure

Fig. 6 CPT results (After Toda et al. 2024)

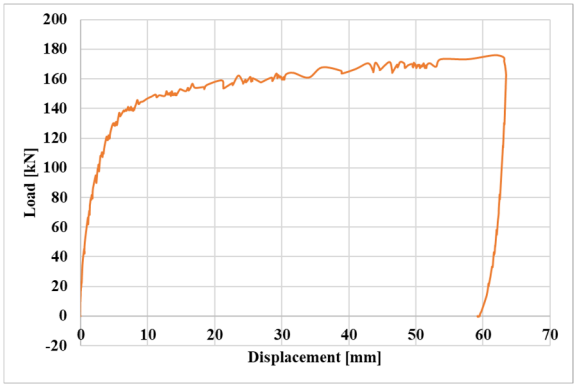

(a) Vertical loading

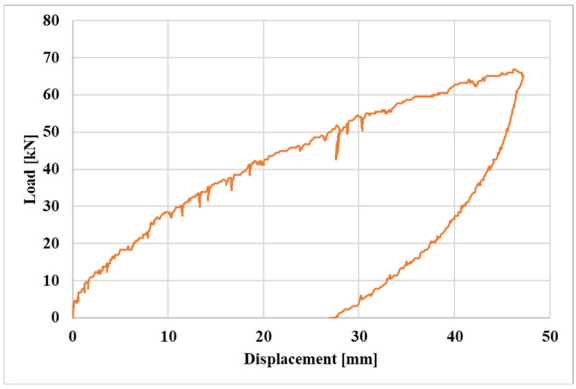

(b) Horizontal loading

Fig. 7 Pretest loading results for r_u= 0 (Toda et al. 2024)

where R_f is the friction ratio, γ_w is the unit weight of water and P_a is the atmospheric pressure.

Various correlations exist linking the friction angle (ϕ') to the CPT parameters. Robertson and Campanella (1983) introduced a correlation for estimating the peak friction angle in sands. Additionally, Kulhawy and Mayne (1990) presented an alternative relationship specifically for the friction angle (ϕ') of sands, formulated as **Eq. (2)** below.

$$\phi' = 17.6 + 11 \log Q_{tn} \tag{2}$$

Where Q_{tn} is the normalized cone resistance which can be obtained from **Eq. (3)** below.

$$Q_{tn} = \left(\frac{q_t - \sigma_{vo}}{P_a}\right)\left(\frac{P_a}{\sigma'_{vo}}\right)^n \tag{3}$$

Where q_t is the corrected cone resistance, σ_{vo} is the vertical total stress, σ'_{vo} is the vertical effective stress, P_a is the atmospheric pressure, and n is a coefficient

varying with soil type and stress level.

The relationship between Young's modulus of soil and the CPT results has been investigated by Robertson (2009). Robertson (2009) proposed an estimation for the soil Young's modulus using **Eq. (4)** below.

$$E = \alpha_E(q_t - \sigma_{vo}) \quad (4)$$

Where q_t is the corrected cone resistance and σ_{vo} is the vertical total stress at a given depth and given r_u. The coefficient α_E can be obtained from **Eq. (5)** below.

$$\alpha_E = 0.015[10^{0.55I_c+1.68}] \quad (5)$$

Where I_c is the Soil Behavior Type Index.

The profiles of soil parameters, including unit weight, frictional angle, and Young's modulus, were determined using the formulae mentioned above for each value of (r_u), as illustrated in **Fig. 8**. The Young's modulus exhibited a significant increase with depth, while the unit weight and frictional angle remained almost constant with increasing depth. The results indicate that an increase in r_u leads to a decrease in all soil parameters. Although the decrease in unit weight and frictional angle could be disregarded, the reduction in Young's modulus is notable. Notably, when (r_u= 0.9), the calculated unit weight appears unreasonable (**Fig. 8a**). The unit weight, being dependent on the friction ratio according to **Eq. (1)**, coupled with the fact that at (r_u = 0.9), the friction is zero (**Fig. 6**), explain the unreasonability of the unit weight in **Fig. 8a** for (r_u= 0.9). Corrections for the unit weight, frictional angle, and Young's modulus at (r_u= 0.9) are proposed in this study, and the correction method will be elaborated upon in the subsequent section. The corrected values are also presented in **Fig. 8**.

4. Investigation of the effect of liquefaction on CPT data and soil parameters

The investigation delves into the impact of liquefaction on both the CPT results and soil parameters, exploring the variations with changes in r_u. Average values for each parameter were calculated at various depths under different values of r_u. The ratios considered for investigation include the corrected cone resistance ratio (R_{q_t}), sleeve friction ratio (R_{f_s}), unit weight ratio (R_γ), the

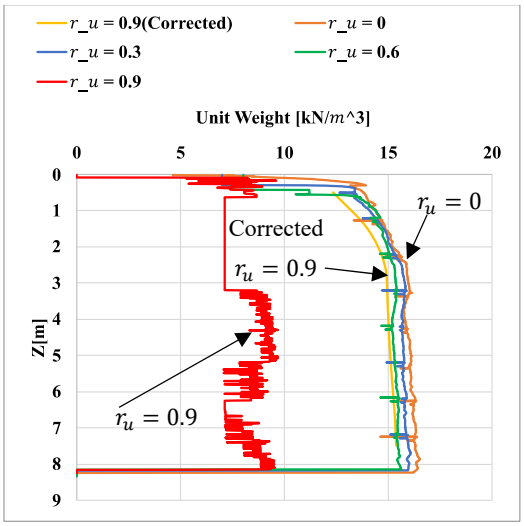

(a) Unit weight

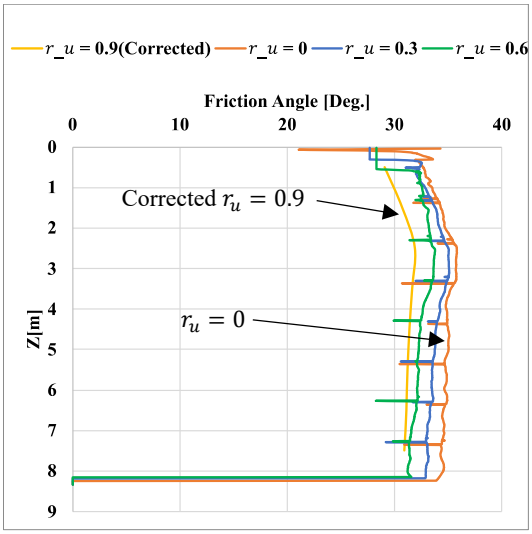

(b) Internal frictional angle

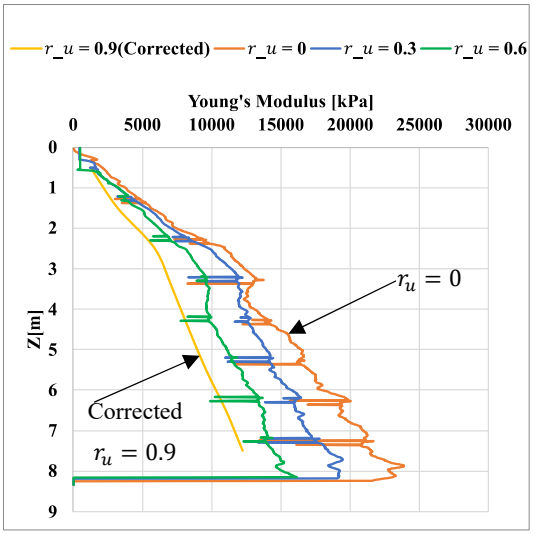

(c) Young's modulus

Fig. 8 Estimated soil parameters from CPT results

internal friction angle ratio (R_φ) and the Young's modulus ratio (R_E). Each ratio is defined as the parameter's value at a specific r_u value relative to its value at $r_u = 0$. The results of these ratios were plotted against r_u, indicating a general trend despite depth-dependent variations.

Fig. 9 illustrates the corrected cone resistance ratio (R_{q_t}) and sleeve friction ratio (R_{f_s}). The corrected cone resistance decreases linearly with increasing r_u, while sleeve friction decreases linearly up to $r_u = 0.6$ and then drops abruptly to zero at $r_u = 0.9$.

Fig. 10 presents the unit weight ratio (R_γ), internal friction angle ratio (R_φ), and Young's modulus ratio (R_E). These parameters show a linear decrease with increasing r_u, with the unit weight decrease considered negligible. The unit weight's sudden decrease at $r_u = 0.9$ is mainly due to the nearly zero value of sleeve friction, which is thought to be related to soil fluidization around the CPT cone, causing water to push soil particles apart, increasing their distance from each other. Hence, in the estimation of the liquefaction effect on sleeve friction (f_s) and unit weight (γ), the values of sleeve friction ratio (R_{f_s}) and unit weight ratio (R_γ) at $r_u = 0.9$ were neglected (see **Fig. 9 (b)** and **Fig. 10 (a)**).

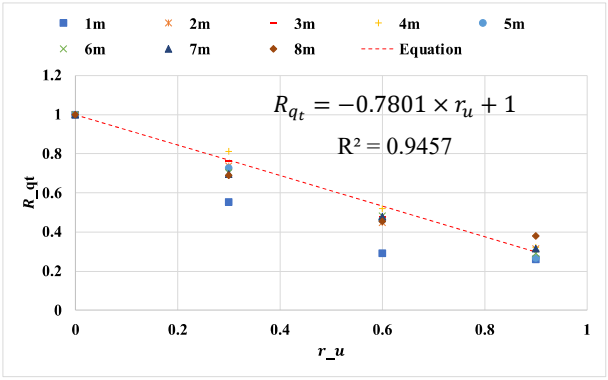

(a) Cone resistance ratio (R_{q_t})

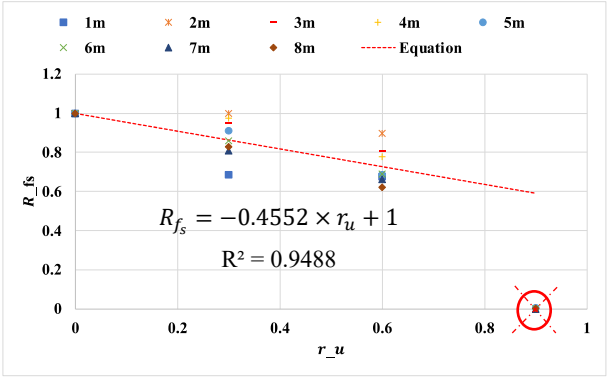

(b) Sleeve friction ratio (R_{f_s})

Fig. 9 Effect of liquefaction on CPT results

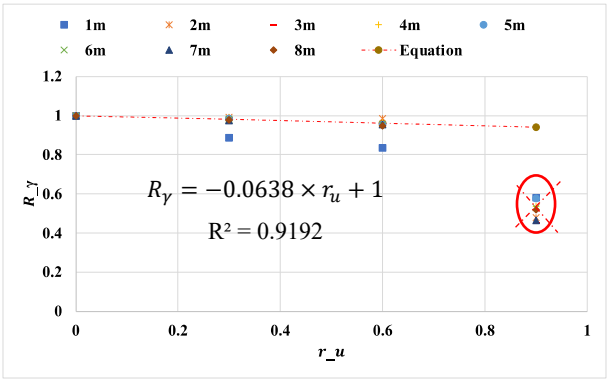

(a) Unit weight ratio (R_γ)

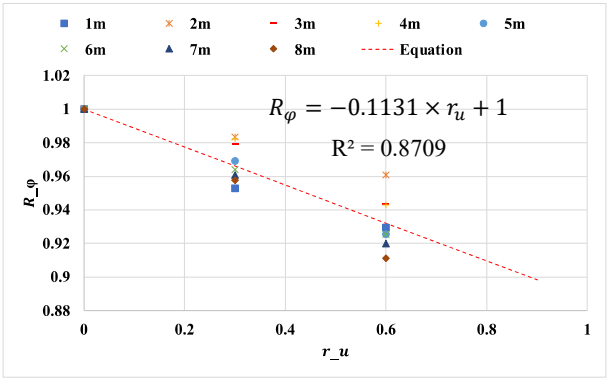

(b) Internal friction angle ratio (R_φ)

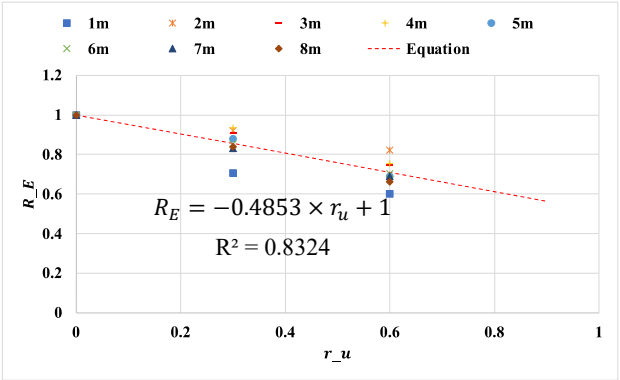

(c) Young's modulus ratio (R_E).

Fig. 10 Effect of liquefaction on soil parameters

Formulae (**Eq. (6)** to **Eq. (10)**) are proposed to express the liquefaction effect on CPT cone resistance (q_t), CPT sleeve friction (f_s), unit weight (γ), internal friction angle (φ), and Young's modulus (E). These formulations capture the relationship between each parameter and r_u.

$$q_t = q_{t0} R_{q_t} = q_{t0}(-0.7801 \times r_u + 1) \quad (6)$$

$$f_s = q_{s0}R_{f_s} = q_{s0}(-0.4552 \times r_u + 1) \quad (7)$$

$$\gamma = \gamma_0 R_\gamma = \gamma_0(-0.0638 \times r_u + 1) \quad (8)$$

$$\varphi = \varphi_0 R_\varphi = \varphi_0(-0.1131 \times r_u + 1) \quad (9)$$

$$E = E_0 R_E = E_0(-0.4853 \times r_u + 1) \quad (10)$$

Where q_{t0}, q_{f0}, γ_0, φ_0, E_0 are the initial cone resistance, the initial sleeve friction, the initial unit weight, the initial internal friction angle, and the initial Young's modulus when $r_u = 0$.

The corrected values of soil parameters presented in **Fig. 8** were derived using the proposed formulas, **Eq. (8)** for the unit weight (γ), **Eq. (8)** for the internal friction angle (φ), and **Eq. (10)** for the Young's modulus (E).

5. Numerical model

The model geometry and mesh, as depicted in **Fig. 11**, mirror the dimensions of the large-scale Liquefaction apparatus, with the pile extending 7.045 m into the ground. The software employed an automatic setting feature to define outer boundaries and establish boundary constraints, fixing the bottom of the model to restrict movements in all directions. A finer mesh was strategically applied around the pile to accurately capture higher deformations.

Leveraging the equations proposed by Tamboura et al. (2024), Joint element parameters were computed and incorporated between the pile and the ground to accurately simulate soil-pile interaction. This method relies on loading test results. However, due to space constraints, a detailed explanation could not be included in this manuscript.

Two load scenarios were considered: vertical and horizontal. For vertical loading, the load increased incrementally from 0 kN to 200 kN at the pile head. Horizontal loading involved applying loads at a height (h) of 1.5 m, akin to large-scale test conditions, increasing from 0 kN to 100 kN with 10 kN increments.

Soil parameters, derived from **Eq. (8)**, **Eq. (9)**, and **Eq. (10)** in combination with the initial values at $r_u = 0$ in **Fig. 8**, were utilized in conjunction with the pile parameters from **Table 2** for the numerical analysis.

In the case of $r_u = 0$, the joint elements parameters were calculated following the method proposed by Tamboura et al. (2024) based on pretest loading results in **Fig. 7**. For cases with $r_u = 0.3$, $r_u = 0.6$, and $r_u = 0.9$, the joint elements were derived by multiplying those in the $r_u = 0$ case with the respective cone resistance ratio R_{q_t} defined in **Fig. 9(a)**. This approach accounted for the variation in cone resistance under different values of r_u, allowing for a dynamic representation of joint elements that align with the changing soil conditions due to liquefaction effects.

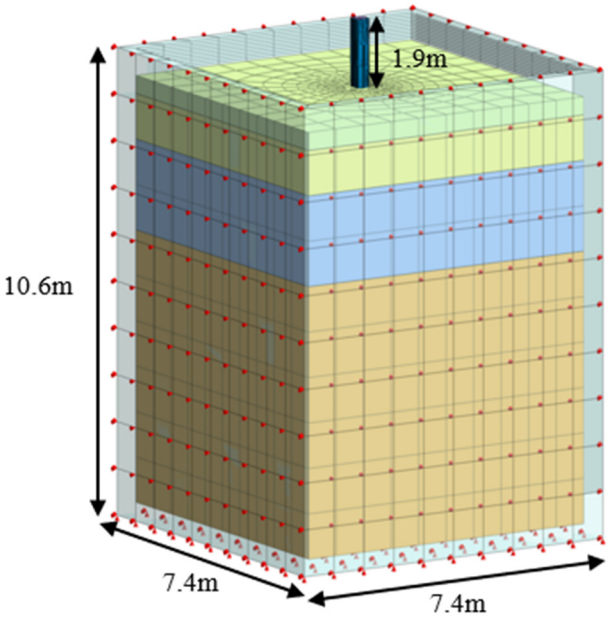

Fig. 11 Geometry, mesh, and boundary conditions

6. Comparison of numerical results and field test results (validation of the numerical model)

The estimated joint element parameters and the soil parameters, obtained with the methods as depicted in section 5, were implemented in MIDAS GTS NX, utilizing the Mohr-Coulomb model, to assess the pile capacity, both vertically and horizontally.

The comparison between the numerical predictions and the results from large-scale tests is depicted in **Fig. 12**. The discrepancy observed between the numerical and large-scale test results is attributed to the used joint elements parameters.

Overall, the numerical outcomes align well with the field test results, indicating the effectiveness of the proposed numerical model and the calculated joint elements in replicating the behavior observed in large-scale loading tests.

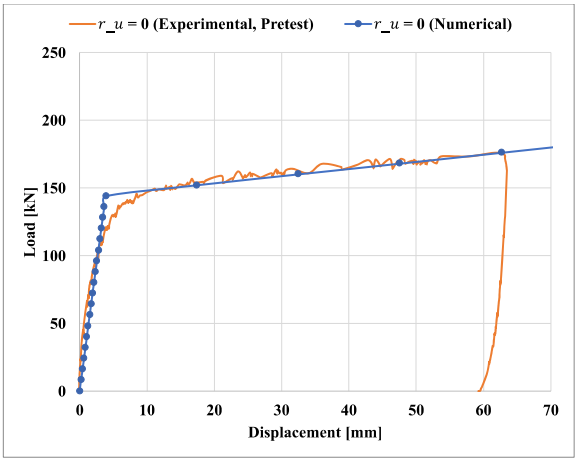

(a) Vertical capacity

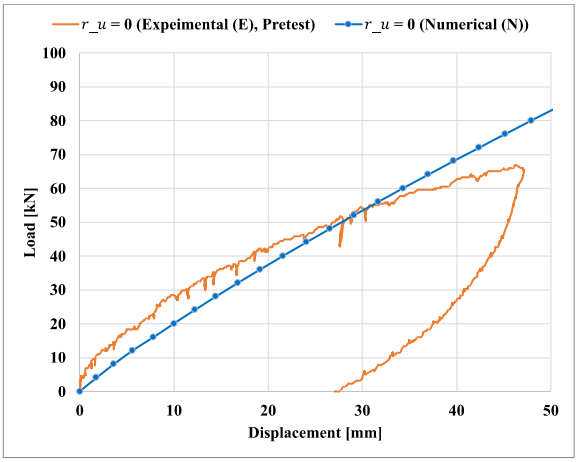

(b) Horizontal capacity

Fig. 12. Validation of the numerical model

7. Influence of the liquefaction on the bearing capacity

The impact of r_u on the bearing capacity of the non-displacement pile was examined through numerical analysis, as illustrated in **Fig. 13**. As anticipated, the bearing capacity exhibits a decrease with the rise in r_u. **Fig. 13** also compares the numerical results (N) with the experimental results (E) of Toda et al. (2024). At r_u = 0, the numerical result aligns with the pretest experimental findings of Toda et al. (2024). However, the experimental results following the pretest show limited improvement in the case of vertical capacity. This is believed to be attributed to the reduction in ground stiffness after the pile is removed and reinstalled for subsequent tests. In the experimental study by Toda et al. (2024), the pile was removed after each test, and ground-making was conducted by fully fluidizing the soil before reinstalling the pile at the same location for the subsequent test. It is presumed that after the pretest involving vertical loading, the removal of the pile has softened the ground at the pile installation location, leading to a reduction in vertical capacity. On the other hand, the comparison of numerical results with experimental results for horizontal capacity is deemed acceptable.

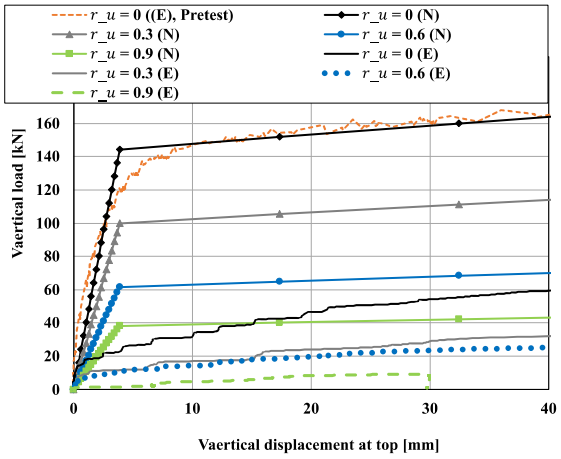

(a) Vertical capacity

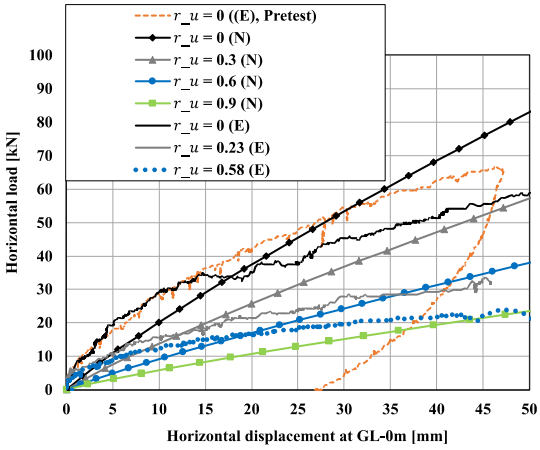

(b) Horizontal capacity

Fig. 13 Influence of liquefaction on the bearing capacity

The findings from numerical analyses are expressed in terms of the bearing capacity ratio (BCR), which is the ratio of the bearing capacity at a specific r_u value to the bearing capacity at r_u = 0. The influence of r_u on the BCR is detailed in **Fig. 14**, demonstrating a linear reduction in bearing capacity with increasing r_u for both vertical and horizontal loading. This trend is consistent with that of the pressed-in pile Willcocks (2021). Based on the trends observed in **Fig. 14**, **Eq. (11)** is proposed as an expression

for the bearing capacity of a non-displacement pile in liquefiable soil, accounting for both vertical and horizontal capacities.

$$q_{ult} = (-0.9 \times r_u + 1)q_0 \quad (11)$$

Where q_0 is the initial vertical or horizontal bearing capacity of non-liquefied ground (r_u = 0).

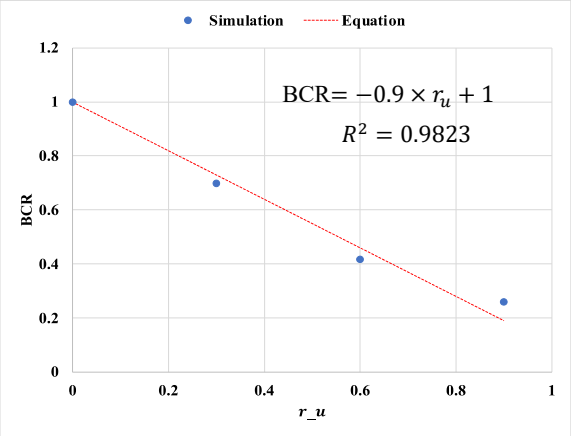

(a) Vertical capacity

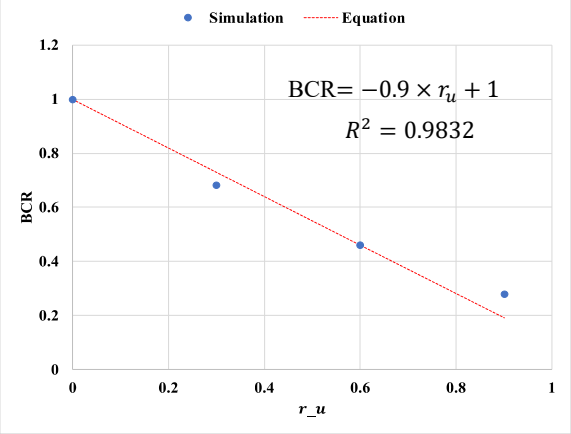

(b) Horizontal capacity

Fig. 14 Correlation between r_u and BCR in numerical analysis

8. Conclusions

This study provided insights into the influence of liquefaction on soil parameters and CPT results. Through analysis and numerical simulations using MIDAS GTS NX, the research replicated large-scale loading test outcomes. Additionally, the study contributed an equation to estimate the impact of liquefaction on both vertical and horizontal pile capacities. These findings enhance our understanding of soil behavior during liquefaction events and offer practical tools for assessing foundation performance in such conditions. The combination of empirical equations and numerical modeling establishes a comprehensive framework for evaluating the complex interactions between soil and piles in liquefiable ground, contributing to improved geotechnical design practices.

References

Ishihara, Y., Ogawa, N., Eguchi, M., Toda, K., 2023. R&D activities on the structures constructed by the press-in method. IPA Newsletter September 2023, vol.8, issue 3, pp.9-14.

Kulhawy, F.H., and Mayne, P.H., 1990. Manual on estimating soil properties for foundation design, Report EL-6800 Electric Power Research Institute, EPRI, August 1990.

Robertson, P. K., 2009. Interpretation of cone penetration tests–a unified approach. Canadian Geotech. J., 46(11), PP. 1337–1355.

Robertson, P.K., and Cabal, K.L., 2010. Estimating soil unit weight from CPT. 2nd International Symposium on Cone Penetration Testing, Huntington Beach, CA, USA, May 2010.

Robertson, P.K., and Campanella, R.G., 1983a. Interpretation of cone penetration tests – Part I (sand). Canadian Geotechnical Journal, 20(4):718-733.

Robertson, P.K., and Campanella, R.G. 1983b. Interpretation of cone penetration tests – Part II (clay). Canadian Geotechnical Journal, 20(4): 734-745.

Tamboura, H. H., Ishihara, Y., Ogawa, N., 2024. Numerical Investigation of Bearing Capacity of Pressed-in Piles for Earth-Based Innovations and Geotechnical Strategies for Construction Projects on the Moon. Proceedings of 3rd International Conference on Press-in Engineering 2024, Singapore.

Toda, K., Mori, A., Ishihara, Y., Eguchi, M., Tamboura, H., H., Pasha, S., M., K., Haigh, S., K., Burakowski, A., 2024. Investigation into geotechnical parameters of liquefied sand by static pile load tests, cone penetration tests and pressuremeter tests. Proceedings of 3rd International Conference on Press-in Engineering 2024, Singapore.

Willcocks, F. 2021. The vertical and horizontal performance of pressed-in tubular piles in liquefied ground. M.Eng. Thesis, University of Cambridge, 52p.